Journal of Virology

The Coronavirus Endoribonuclease Nsp15 Interacts with Retinoblastoma Tumor Suppressor Protein

Kanchan Bhardwaj, Pinghua Liu, Julian L. Leibowitz and C. Cheng Kao

J. Virol. **2012, 86(8):4294. DOI: 10.1128/JVI.07012-11.**
Published Ahead of Print 1 February 2012.

JVI Journals.ASM.org

The Coronavirus Endoribonuclease Nsp15 Interacts with Retinoblastoma Tumor Suppressor Protein

Kanchan Bhardwaj,[a] Pinghua Liu,[b] Julian L. Leibowitz,[b] and C. Cheng Kao[a]

Department of Molecular and Cellular Biochemistry, Indiana University, Bloomington, Indiana, USA,[a] and Department of Microbial and Molecular Pathogenesis, Texas A&M Health Science Center College of Medicine, College Station, Texas, USA[b]

Coronaviruses encode an endoribonuclease, Nsp15, which has a poorly defined role in infection. Sequence analysis revealed a retinoblastoma protein-binding motif (LXCXE/D) in the majority of the Nsp15 of the severe acute respiratory syndrome coronavirus (SARS-CoV) and its orthologs in the alpha and beta coronaviruses. The endoribonuclease activity of the SARS-CoV Nsp15 (sNsp15) was stimulated by retinoblastoma protein (pRb) *in vitro*, and the two proteins can be coimmunoprecipitated from cellular extracts. Mutations in the pRb-binding motif rendered sNsp15 to be differentially modified by ubiquitin in cells, and cytotoxicity was observed upon its expression. Expression of the sNsp15 in cells resulted in an increased abundance of pRb in the cytoplasm, decreased overall levels of pRb, an increased proportion of cells in the S phase of the cell cycle, and an enhanced expression from a promoter normally repressed by pRb. The endoribonuclease activity of the mouse hepatitis virus (MHV) A59 Nsp15 was also increased by pRb *in vitro*, and an MHV with mutations in the LXCXE/D-motif, named vLC, exhibited a smaller plaque diameter and reduced the virus titer by ~1 log. Overexpression of pRb delayed the viral protein production by wild-type MHV but not by vLC. This study reveals that pRb and its interaction with Nsp15 can affect coronavirus infection and adds coronaviruses to a small but growing family of RNA viruses that encode a protein to interact with pRb.

Coronaviruses can cause diseases in humans, including severe acute respiratory syndrome (SARS), which had an associated fatality rate of ~10% during the 2002–2003 outbreak (17, 37). Coronaviruses are also of interest for their ~30-kb positive-strand genomes and novel mechanisms to express and process this large RNA (12, 22, 25). All known members of nidovirus family that includes coronaviruses encode an endoribonuclease, with the exception of Nam Dinh virus (33). A recombinant endoribonuclease of the SARS-CoV (Nsp15) cleaves RNAs immediately 3′ of uridylates. This activity is stimulated by Mn^{2+} but not by other divalent metals, such as Mg^{2+} (2). Furthermore, cleavage occurs through the formation of a 2′-3′ cyclic phosphodiester product in a mechanism identical to that of RNase A (4). Crystal structures of the SARS-CoV and the mouse hepatitis virus (MHV) Nsp15 have been reported, and both proteins form hexamers in solution (3, 36, 42).

Mutations in the active site of Nsp15 that apparently abolish endoribonuclease activity *in vitro* reduce viral infectivity by up to 2 logs (20, 35). However, some mutations outside of the active site are reported to have a larger effect on virus viability, suggesting that Nsp15 has role(s) in coronavirus infection apart from its function as an endoribonuclease (18, 20). In addition, the SARS-CoV Nsp15 was identified in a screen for viral proteins that can suppress apoptosis demonstrating that SARS-CoV Nsp15 can affect host cell processes (24).

In order to better understand the role of SARS-CoV Nsp15 in viral infection, we searched for motifs within sNsp15 and identified a sequence diagnostic for proteins that can bind the retinoblastoma protein (pRb). This motif was originally identified in oncoproteins encoded by DNA tumor viruses that can sequester pRb and prevent the repression of genes needed for DNA replication (5, 10, 11, 41). Some RNA viruses are also known to interact with pRb. Hepatitis C virus (HCV) can downregulate pRb and enhance cell cycle progression (27). Intriguingly, the HCV RNA-dependent RNA polymerase NS5B binds pRb and targets it for ubiquitination and proteasomal degradation (27, 28). The measles virus also has a similar mechanism (30). The rubella virus protein Nsp90 has also been shown to interact with pRb (1) and affect virus replication (13). Although RNA viruses do not require the host DNA replication machinery, their interaction with pRb could result in alteration of the metabolic state of the cell and affect virus infection (31, 34, 38).

In the present study, we examined the functional relevance of the identified pRb-binding (LXCXE/D) motif on Nsp15 and studied the effects of Nsp15 on pRb and its functions. Further, we examined the significance of pRb and its interaction with Nsp15 for MHV infection in cultured cells.

MATERIALS AND METHODS

Cells and viruses. DBT cells derived from a mouse brain tumor were maintained at 37°C with 5% CO_2 in Dulbecco modified Eagle medium (DMEM) supplemented with 10% bovine calf serum (HyClone, Logan, UT; catalog no. SH30072.03). Baby hamster kidney-21 cells expressing the MHV receptor (BHK-R) were grown in minimal essential medium supplemented with 10% bovine calf serum, 10% tryptose phosphate broth, and G418 (800 μg/ml). Murine fibroblast cells (L2) were grown in DMEM supplemented with 10% bovine calf serum and maintained at 37°C under 3% CO_2. NIH 3T3 cells were grown at 37°C under 5% CO_2 in DMEM with 4 mM L-glutamine, 1.5 g sodium bicarbonate/liter, and 4.5 g of glucose (American Type Culture Collection; catalog no. 30-2002)/liter, and 10% calf serum. MHV A59 and mutant derivatives were propagated in the DBT cell line. 293T and Huh-7 cells were maintained at 37°C and 5% CO_2 in 10% bovine calf serum containing, respectively, high-glucose DMEM

Received 5 December 2011 Accepted 26 January 2012
Published ahead of print 1 February 2012
Address correspondence to Kanchan Bhardwaj, kanchan@indiana.edu.

doi:10.1128/JVI.07012-11

with GlutaMAX (Invitrogen, Inc.; catalog no. 10569) and low-glucose DMEM (Invitrogen, Inc.; catalog no.11885).

Protein purification. Wild-type (WT) and mutant Nsp15 proteins containing a His_6 tag at their respective N termini were expressed in *Escherichia coli* Rosetta(DE3) pLys strain and purified by using metal ion affinity chromatography, followed by a Mono-Q and a gel filtration column, as described previously (2). The purified proteins were stored in 50 mM Tris (pH 7.9)–300 mM NaCl–1 mM dithiothreitol (DTT)–50% (vol/vol) glycerol at −20°C. The pRb_{AB} (spanning AB domains of pRb; amino acids 380 to 787) was expressed as a glutathione *S*-transferase (GST) fusion in *E. coli* BL21(DE3) cells. Induction was carried out at 22°C for 16 h. The protein was purified from cell lysate generated by sonication in 1× phosphate-buffered saline (PBS) containing 10 mM β-mercaptoethanol. The lysate was passed through a glutathione-Sepharose 4 Fast Flow (GE Healthcare) affinity column, and protein was eluted with restriction-grade thrombin (Novagen). Eluted fractions were further passed through a Superdex 200 10/300 GL (Pharmacia) gel filtration column equilibrated with buffer (10 mM Tris [pH 7.5], 150 mM NaCl, 10% glycerol, 5 mM DTT). Protein concentrations were determined from the absorbance at 280 nm, and aliquots of the purified protein were stored in the same buffer at −80°C.

Nsp15 endoribonuclease assay. The substrate used in this assay is four nucleotides in length and has a 5′ fluorophore carboxyfluorescein (FAM) and a 3′ tetramethyl rhodamine that quenches FAM fluorescence (Integrated DNA Technologies) when the substrate is intact. The cognate nucleotide is a ribonucleotide, whereas the other three are deoxyribonucleotides. The fluorescence released by incubation of purified Nsp15 protein with the substrate was measured in real time using an LS55 spectrometer (Perkin-Elmer, Inc.) as described earlier (4).

Coimmunoprecipitation assays. 293T cells were grown to ~80% confluence and, using Lipofectamine 2000 reagent (Invitrogen, Inc.), they were transfected with plasmids to coexpress pRb_{ABC} (spanning ABC domains of pRb) and either sNsp15 containing a C-terminal hemagglutinin (HA) tag ($sNsp15_{HA}$ [kindly provided by Ralph Baric]) or LC mutant tagged similarly at the C terminus (LC_{HA}). At 48 h posttransfection, the cells were lysed in cell lysis buffer (20 mM Tris [pH 7.5], 150 mM NaCl, 10 mM EDTA, 1% NP-40, 10% glycerol), and extracts were prepared as described earlier (28). Extracts (500 μg) clarified by centrifugation at 10,000 × *g* for 30 min at 4°C were mixed with anti-pRb monoclonal antibody 4H1 (Cell Signaling Technology; catalog no. 9309) at a 1:100 dilution. After a 4 h of incubation at 4°C, 20 μl of a slurry of pre-equilibrated Protein A/G Plus-agarose (Santa Cruz Biotechnology, Inc.; catalog no. sc-2003) was added to the extracts, followed by incubation overnight at 4°C with rocking. The resin was washed twice with cell lysis buffer and collected by centrifugation. The resin was then resuspended in 1× electrophoresis sample buffer to elute proteins for SDS-PAGE and Western blot analysis. The Western blots were probed using anti-HA antibody (Abcam, Inc.; catalog no. ab9134) or anti-ubiquitin monoclonal antibody P4D1 (Santa Cruz Biotechnology, Inc.; catalog no. sc-8017).

Cell viability and fluorescence-activated cell sorting (FACS) analysis. Nsp15-transfected Huh7 cells were harvested by trypsinization. They were washed with PBS twice and then with 1× annexin V binding buffer once. The cells were stained with annexin V-fluorescein isothiocyanate (FITC) according to the provider's recommendations (eBioscience, Inc.; catalog no. 88-8005). Dead cells were stained with 7-AAD (BD Pharmingen; catalog no. 51-68981E) for 5 min at room temperature. Data were collected on a FACSCalibur (BD Biosciences, San Jose, CA) and analyzed by using WinMDI software.

Fluorescence microscopy. Expression vector or sNsp15 ($sNsp15_{HA}$, LC_{HA}, or $H249A_{HA}$)-transfected Huh7 cells were seeded on eight-well glass chamber slides. After being washed with PBS, cells were fixed with 4% paraformaldehyde at room temperature for 15 min. After three additional washes with PBS, the cells were permeabilized with ice-cold 100% methanol at −20°C for 10 min, rinsed with PBS for 5 min, and incubated with blocking buffer (5% normal fetal bovine serum and 0.5% Triton X-100 in PBS) for 1 h at room temperature. Anti-HA and anti-pRb (4H1) antibodies were used to detect Nsp15 and pRb, respectively, at a 1:200 dilution using antibody dilution buffer (1% bovine serum albumin and 0.5% Triton X-100 in PBS). After three washes with PBS-T (0.5% Tween 20 in PBS), the slides were incubated with anti-goat IgG secondary antibody conjugated with Texas Red to detect Nsp15 or anti-rabbit immunoglobulin secondary antibody conjugated with FITC to detect pRb for 1 h at room temperature (at 1:200 dilution). The slides were washed with PBS-T three times and mounted in Vectashield mounting medium (Vector Laboratories). The images were obtained on Leica TCS SP5 scanning confocal microscope with an HCX PL APO Lambda Blue 63X1.4 oil objective lens (Leica Microsystems). Excitation was at 20% Hz, and the image resolution was 512 × 512 pixels. Images were analyzed using Leica Application Suite 2.02.

Colony formation assay. NIH 3T3 cells were seeded in six-well plates at 0.25×10^6 cells per well and transfected either with pUNO vector alone or with sNsp15 expressed from pUNO vector using Lipofectamine 2000 reagent. At 24 h after transfection, each well of cells was transferred into a 10-cm culture dish and allowed to grow in medium containing 10 μg of blasticidin/ml. The cells were fed with fresh medium containing 10 μg of blasticidin/ml every 3 days. Four weeks later, the colonies were fixed in methanol and stained with 1% crystal violet prepared in 20% ethanol.

Cell cycle analysis. NIH 3T3 cells were transfected in 10-cm culture dishes either with vector alone or vectors expressing WT sNsp15 using Lipofectamine 2000 reagent. The cells were harvested 36 h posttransfection, washed with PBS, and resuspended at 2×10^6 cells per ml of cold PBS. The cell suspension was added dropwise to an equal volume of cold absolute ethanol with continuous vortexing to fix the cells. After an overnight incubation at 4°C, cellular DNA was stained with 500 μg of propidium iodide (Invitrogen, Inc.)/ml prepared in PBS containing 0.1% (vol/vol) Triton X-100 (Sigma-Aldrich) and 2 mg of DNase-free RNase A (Sigma-Aldrich) at 37°C for 15 min in the dark. The samples were filtered through nylon mesh to remove cell clumps and analyzed by using a FACSCalibur flow cytometer (BD Biosciences, San Jose, CA). A total of 15,000 cells were analyzed using ModFitLT V3.0.

Luciferase reporter assay. NIH 3T3 cells were plated in Costar White 96-well plates at 4×10^4 cells per well for transfection. At approximately 60 to 80% confluence, they were cotransfected with 5 ng of the reporter plasmid phRL-TK (Promega) or phRL-CMV (Promega), along with indicated amounts of either the expression vector for $H249A_{HA}$ sNsp15 or with the expression vector alone. The cells were incubated for 48 h to allow expression from the plasmids. The Dual-Glo luciferase assay system (Promega), was used to quantify luminescence with the FLU-Ostar Optima Plate Reader (BMG Labtech). The fold induction was calculated by normalizing the data with vector control.

Mutant MHV construction. The MHV-A59 1000 reverse-genetics system (43) was used to recover viruses with mutations in mNsp15. Briefly, a 3.4-kb BamHI-HpaI fragment spanning the region of interest in mNsp15 from the F plasmid (43) was amplified and cloned into the pGEM-T vector as described previously (20). The LC mutation was introduced into mNsp15 using a QuikChange II site-directed mutagenesis kit (Stratagene) according to the manufacturer's instructions. The sequence of BamHI-HpaI fragment carrying the mutations in mNsp15 was determined to confirm that the desired sequences were obtained. The BamHI-HpaI fragment containing the mutations was excised and religated into plasmid F digested with the same enzymes. The ligation products were then transformed into the Top10 strain of *E. coli*. The region of the recovered clones between the BamHI and HpaI sites was sequenced again to verify that the desired mutations were recovered. MHV-A59 genomes containing mNsp15 WT and the mutant sequences were generated by ligation of cDNAs followed by *in vitro* transcription and these genomes were then electroporated into BHK-R cells as previously described (43). Cultures were observed for 72 h posttransfection for the development of cytopathic effects or syncytium formation. Virus-infected cultures were then harvested and frozen at −70°C. Mutant viruses were subjected to one

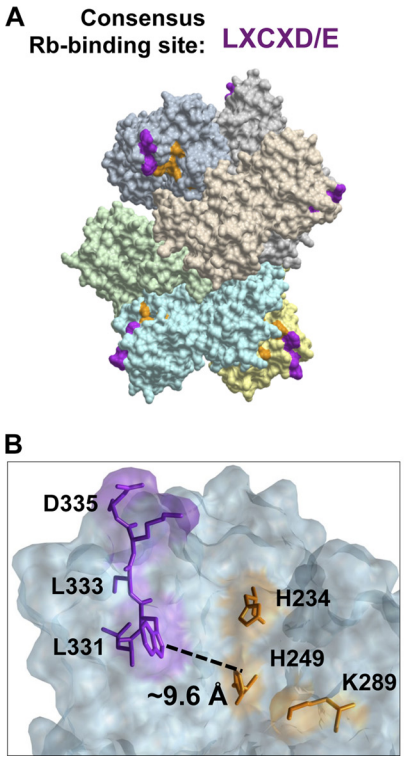

C

Virus	Group	Sequence
Nsp15:		
SARS CoV	Beta	^{331}LWCKD
MHV	Beta	^{359}LWCNE
BCoV	Beta	^{359}LWCND
HCoV OC43	Beta	^{372}LWCND
PheV	Beta	^{372}LWCND
ECoV	Beta	^{363}LWCND
HCoV HKU1	Beta	^{371}LWCND
BatCoV HKU5	Beta	^{348}LWCKD
HCoV 229E	Alpha	^{360}LWCND
PeDV	Alpha	^{325}LWCKD
HCoV NL63	Alpha	^{329}LWCKD
BatCoV HKU8	Alpha	^{324}LWCKD
Scotophilus batCoV 512	Alpha	^{324}LWCKD
Rhinolophus batCoV HKU2	Alpha	^{328}LWCKD
ORF 1a:		
TGEV	Alpha	^{2992}LACYE
IBV	Gamma	^{3440}LFCVD, ^{4409}LFCLE

FIG 1 pRb-binding motif in the SARS-CoV Nsp15 protein and in proteins of other coronaviruses. (A) Localization of the pRb-binding motif (purple) relative to the endoribonuclease catalytic site (orange) on SARS-CoV Nsp15 (sNsp15) hexamer. The structure of SARS-CoV Nsp15 was from Bhardwaj et al. (3) (Protein Data Bank: 2RHB). The Nsp15 protein was from the Urbani isolate (GenBank accession no. AY278741). (B) Close-up view showing orientation and distance between the residues of pRb-binding motif (purple) and the endoribonuclease catalytic site (orange) on sNsp15. (C) Sequence alignment of the pRb-binding motif in the Nsp15 orthologs. The following list gives the names of the viruses examined for the presence of the pRb-binding motif, followed by the GenBank accession numbers in parentheses: SARS-CoV (NC_004718), MHV (NC_001846), BCoV (AF391542), HCoV OC43 (ay391777), PheV (YP_459949.1), EcoV (YP_001671996), HCoV HKU1 (ay597011), BatCoV HKU5 (ef065509) HCoV 229E (NC_002645), PeDV (AEQ55003), HCoV NL63 (ABE97136), BatCoV HKU8 (ACA52170), *Scotophilus* batCoV (YP_001351683), and *Rhinolophus* batCoV HKU2 (ABQ57231). The residue number of the first residue of the motif in the proteolytically processed Nsp15 or Nsp15 ortholog is shown. Several nidoviruses lack the Rb-binding motif within the Nsp15 ortholog but contain such a motif within other replication-associated proteins. Two examples of the motifs within the ORF1a of TGEV (NC_002306) and IBV (NC_001451) are shown.

round of plaque purification and amplified once in DBT cells to generate stocks. The sequences of recovered viruses corresponding to the 5′ and 3′ UTRs, as well as the portions encoding mNsp15 mutant proteins, were amplified by reverse transcription-PCR, followed by direct sequencing of the amplified products.

MHV growth and plaque formation assay. Growth curves for MHV were determined in L2 cells seeded in 96-well plates and grown in 0.1% serum supplemented growth medium for 48 h. The cells were infected at a multiplicity of infection (MOI) of 1.0 with mNsp15 mutant (vLC) or WT MHV-A59 for 1 h. The cells were washed to remove the unattached virus that was remaining in the medium. Cultures were fed and further incubated until 0, 10, 12, 16, 24, 28, and 30 h postinfection (hpi), at which time they were frozen at −70°C. Triplicate samples were obtained for all time points. Virus production was quantified by plaque assays on monolayers of L2 cells.

pRb overexpression and analysis of the MHV nucleocapsid (N) protein. DBT cells (2.5×10^5 per well) were seeded onto 12-well plates and transfected with either the expression vector (pUNO) or vector expressing pRb ABC domains (pRb_{ABC}) using Lipofectamine 2000 reagent. At 6 h after transfection, the cells were washed and fed with fresh medium. At ~36 h after transfection, the cells were infected with either WT or vLC MHV at an MOI of ~5.0. At 4, 6, 8, 10, and 12 hpi, the medium was removed, and the cells were lysed with 1× electrophoresis buffer. An equal amount of lysate was electrophoresed on 4 to 12% NuPAGE Bis-Tris gels (Invitrogen, Inc.) and transferred to polyvinylidene difluoride membranes for Western blotting. Protein was detected with anti-MHV N protein monoclonal antibodies and horseradish peroxidase-conjugated anti-mouse secondary antibody (Santa Cruz Biotechnology) and the Amersham ECL Plus Western detection system according to the manufacturer's recommendations. After detection of the MHV N protein, the blots were stripped with Tris (pH 7.0) containing 2% SDS and 50 mM DTT for 2 h at 37°C and probed for pRb using anti-pRb monoclonal antibody 4H1.

RESULTS

Coronavirus Nsp15 orthologs interact with pRb. A search for motifs within the SARS-CoV Nsp15 (sNsp15) identified the LXCXE/D motif that is characteristic for proteins that bind to the retinoblastoma protein (pRb) (26). The motif lies within 10 Å of the endoribonuclease active site of sNsp15 and is exposed on the protein surface (Fig. 1A and B). The same motif was found in the Nsp15 orthologs of alpha and beta coronaviruses, and a partial list is shown in Fig. 1C. The LXCXE/D motif, however, was not present in all of the Nsp15 orthologs of all coronaviruses. For example, the Nsp15 orthologs of transmissible gastroenteritis virus (TGEV; an alpha coronavirus), infectious bronchitis virus (IBV, a gamma coronavirus), and turkey coronavirus (TCoV, a gamma coronavirus) all lacked this motif. Toroviruses such as equine torovirus (EToV) and arteriviruses such as LDC-V also lacked a recognizable LXCXD motif in Nsp15. Interestingly, an LXCXD motif is present in other 1ab proteins. For example, the motif is found in

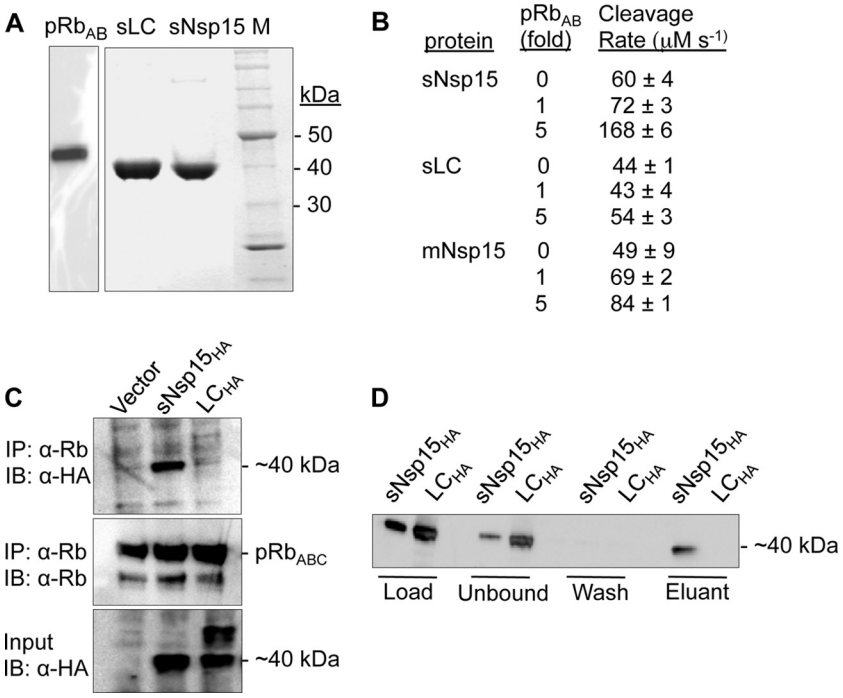

FIG 2 Interaction between pRb and Nsp15. (A) SDS-PAGE analysis of the purified proteins—human pRb_{AB} (pRb-spanning AB domains), sLC (pRb-binding mutant of SARS-CoV Nsp15), and sNsp15 (SARS CoV Nsp15)—used in the study. (B) Effect of pRb_{AB} addition on the endoribonuclease activity of (sNsp15), sLC, and MHV Nsp15 (mNsp15). (C) Coimmunoprecipitation of $sNsp15_{HA}$ (HA-tagged sNsp15) with coexpressed pRb_{ABC} (pRb-spanning ABC domains) from cellular lysates. The LC_{HA} (HA-tagged pRb-binding mutant of sNsp15) and vector are shown as specificity controls. Antibodies used for immunoprecipitation (IP) and immunoblotting (IB) are shown on the left. The expected position of Nsp15 migration on gel (~40 kDa) is shown on the right. (D) Western blot analysis of various fractions collected upon passing $sNsp15_{HA}$- or LC_{HA}-expressing cellular lysates through a GST-pRb_{AB}-bound glutathione-agarose column. Anti-HA antibodies were used for the detection of Nsp15 (molecular mass, ~40 kDa).

the 1a proteins of TGEV 1a and IBV (Fig. 1C). The functional relevance of these motifs in other coronaviruses will not be addressed in this work.

We speculate that the pRb would bind sNsp15 and affect its endoribonuclease activity. To test this, we produced a recombinant truncated form of human pRb (pRb_{AB}) that is sufficient to bind to the LXCXE/D motif (23) (Fig. 2A). We also expressed and purified the WT and a mutant sNsp15 named sLC that has alanine substitutions of L331 and C333 of the LXCXD motif (mutated residues underlined) (Fig. 2A). Size-exclusion chromatography revealed that both WT sNsp15 and the sLC mutant eluted predominantly as hexamers, a feature necessary for Nsp15 endoribonuclease activity (16; data not shown). Furthermore, the sLC mutant preferentially cleaved a tetranucleotide fluorophore substrate containing a cognate uridylate, and its activity was dependent on Mn^{2+} similar to the WT sNsp15, demonstrating that the mutation did not affect endoribonuclease activity (data not shown). In the presence of increasing concentrations of pRb_{AB}, the rates of substrate cleavage by WT sNsp15 increased proportionally, while cleavage by the sLC mutant was not particularly affected ($n = 3$, $P < 0.0001$; Fig. 2B). The WT MHV Nsp15 (mNsp15) also exhibited increased endoribonuclease activity in the presence of pRb (Fig. 2B). These results show that sNsp15 endoribonuclease activity does not require pRb, but that there may be interactions between the proteins.

To determine whether sNsp15 can interact with pRb in cells, we ectopically coexpressed human pRb spanning the ABC domains (pRb_{ABC}), along with either an HA-tagged sNsp15 ($sNsp15_{HA}$) or the mutant with alanine substitutions of L331 and C333 in the LXCXD (mutated residues underlined) motif (LC_{HA}) in 293T cells. The cell lysates were immunoprecipitated with monoclonal antibody to pRb and then subjected to Western blot to detect the HA tag in Nsp15. Notably, LC_{HA} expression in cells was found to be lower than that of $sNsp15_{HA}$ (see below for additional examination of the LC_{HA} protein). Therefore, we used four times the amount of LC_{HA}-expressing lysate to adjust for comparable amounts of WT and LC sNsp15 for immunoprecipitation. The volume for WT $sNsp15_{HA}$ was adjusted similarly with vector-transfected cell lysate. WT $sNsp15_{HA}$ was found to coimmunoprecipitate with pRb but not the LC_{HA} mutant (Fig. 2C). In an independent assay, purified recombinant GST-tagged pRb (pRb-GST) was bound to glutathione-Sepharose resin and incubated with cell lysates expressing either $sNsp15_{HA}$ or LC_{HA}. After extensive washes, the bound materials were eluted and subjected to Western blot analysis. WT $sNsp15_{HA}$ but not the LC_{HA} mutant was readily detected in the bound material (Fig. 2D). These results show that Nsp15 binds to pRb in cells and that the LXCXD/E motif contributes to the binding. This encouraged us to determine the consequences of pRb-Nsp15 interaction.

LC_{HA} mutant accumulates to lower levels, is differentially modified, and exhibits increased apoptosis and cell death. We consistently observed that the extracts from transiently transfected cells contained lower amounts of LC_{HA} protein than did the $sNsp15_{HA}$ (Fig. 3A). Furthermore, on denaturing polyacrylamide gels, the LC_{HA} protein migrated as multiple bands, both larger and smaller than the molecular mass of the Nsp15 monomer that are

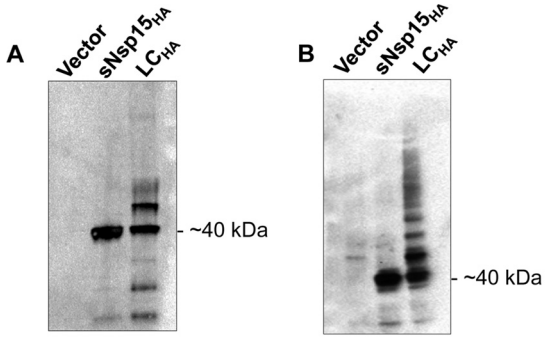

C

Nsp15	Live	Apoptotic	Dead	Dead+Apoptotic
$sNsp15_{HA}$	82 ± 2	5.2 ± 0.8	5.5 ± 0.6	7.1 ± 1.4
LC_{HA}	66 ± 4	8.0 ± 1.1	9.9 ± 0.9	15.7 ± 2.1
$H249A_{HA}$	80 ± 4	5.0 ± 1.3	5.4 ± 1.2	9.5 ± 0.7

FIG 3 Properties of pRb-binding mutant Nsp15. (A) Western blot analysis of lysates from vector-, $sNsp15_{HA}$-, or LC_{HA}-transfected 293T cells. Blots were probed with anti-HA antibodies. The expected position of Nsp15 migration on the gel (~40 kDa) is shown. (B) Western blot showing coimmunoprecipitation of ubiquitin with $sNsp15_{HA}$ and LC_{HA} from cell extracts. Vector-transfected cells were used as a control. Anti-HA antibodies were used for immunoprecipitation, and anti-ubiquitin antibodies were used for Western blotting. (C) FACS analysis. A summary of the cells (%) undergoing apoptosis and cell death upon expression of $sNsp15_{HA}$, LC_{HA}, or $H249A_{HA}$ (endoribonuclease mutant of SARS Co-V sNsp15) is presented in the table. The cells were transfected to express $sNsp15_{HA}$, LC_{HA}, or $H249A_{HA}$ (the endoribonuclease mutant of sNsp15) and stained to detect annexin V and DNA with propidium iodide (PI). For data analysis, the cells were divided into four quadrants based on the intensity of the signal from annexin V and PI. The table shows the mean percentages of the cells in each quadrant, and the values were interpreted as follows. The live cells are negative for both annexin V^- PI^- (live), the apoptotic cells are positive for positive for annexin A but negative for PI, the dead cells are negative for annexin V but positive for PI, and the cells that are both apoptotic and dead are positive for both signals.

indicative of covalent modifications as well as degradation (Fig. 2C and 3A). This is in contrast to the $sNsp15_{HA}$, which migrated at the expected monomer molecular mass (~40 kDa) (Fig. 2C and 3A). To test whether LC_{HA} was modified by ubiquitin relative to sNsp15, we coexpressed ubiquitin in the same cells. The cell lysates were immunoprecipitated with anti-HA antibodies, followed by Western blot analysis to detect ubiquitin. Both WT $sNsp15_{HA}$ and LC_{HA} were positive for ubiquitin (Fig. 3B). However, whereas $sNsp15_{HA}$ migrated in one band indicative of a monoubiquitinated form, LC_{HA} existed in a ladder of bands that is expected for a polyubiquitinated protein (Fig. 3B).

We also investigated whether cytotoxicity was a reason for lower accumulation of LC_{HA}. Huh7 cells were transfected with $sNsp15_{HA}$, LC_{HA}, or the endoribonuclease mutant, $H249A_{HA}$. At 36 h posttransfection, the cells were stained with annexin V-FITC and 7-AAD to determine apoptosis and cell death, respectively. FACS analysis showed that the cells transfected to express LC_{HA} had higher levels of apoptosis and cell death compared to $sNsp15_{HA}$- or $H249A_{HA}$-transfected cells ($n = 3$; $P < 0.0001$; Fig. 3C). These results show that when Nsp15 cannot efficiently interact with pRb, it is differentially modified and has cytotoxicity (Fig. 3B and C).

Ectopic expression of Nsp15 alters the cellular distribution of pRb. Coronaviruses replicate in association with cytoplasmic membranes, although some of their proteins can localize to the nucleus (15). We wanted to determine the cellular localization of Nsp15 and pRb. Huh-7 cells were transfected to express $sNsp15_{HA}$, LC_{HA}, or $H249A_{HA}$. Confocal immunofluorescence microscopy images showed that $sNsp15_{HA}$ localizes predominantly in the cell cytoplasm (Fig. 4A). Notably, not all of the cells within an image were successfully transfected. pRb was localized predominantly in the nuclei of cells that were not expressing $sNsp15_{HA}$. However, in cells expressing $sNsp15_{HA}$ or $H249A_{HA}$, pRb was detected both in the cytoplasm and the nucleus (Fig. 4A and B).

To determine whether pRb redistribution requires interaction with Nsp15 via the LXCXE/D motif, we analyzed pRb localization in LC_{HA}-transfected cells. Consistent with the results from Western blots, LC_{HA} was less abundant, and hence the gain was adjusted higher than that for WT $sNsp15_{HA}$ or $H249A_{HA}$. We also identified cells with higher levels of LC_{HA} proteins. Even with these manipulations, preferential redistribution of pRb into the cytoplasm in cells was not detected in cells expressing LC_{HA} (Fig. 4C). Furthermore, we note that LC_{HA} was present at similar levels in both the nucleus and the cytoplasm in a majority of the transfected cells.

To confirm the relocalization of pRb by WT sNsp15, we separated the nuclear and cytoplasmic fractions of cells transfected to express sNsp15 and performed Western blots to detect pRb. An increase in the abundance of pRb was observed in the cytoplasmic fraction in three independent experiments, and representative results are in shown in Fig. 4D. These results show that expression of sNsp15 is correlated with a redistribution of pRb in cells.

Nsp15 affects pRb function. Oncoproteins from DNA tumor viruses can bind pRb and induce NIH 3T3 cells to undergo contact-independent cell growth in a focus formation assay (9, 11, 21, 23, 29, 41). We sought to determine whether sNsp15 had the ability to increase focus formation. NIH 3T3 fibroblasts were transfected to express sNsp15 or empty expression vector. After 4 to 5 weeks of selection, the cells were stained with crystal violet. In four independent experiments, plates containing the cells transfected to express sNsp15 had severalfold higher cell number compared to the cells transfected with the empty vector (Fig. 5A). Cells expressing sLC did not increase colony formation but, due to the pleiotropic effects associated with sLC, it is difficult to interpret these results.

The lack of contact-inhibition in cell growth suggests that sNsp15 interacted with pRb perturbed the regulation of the cell cycle. To examine this directly, NIH 3T3 cells were transfected to express the vector or sNsp15. The amount of DNA in 15,000 cells per sample was quantified using FACS to determine the number of cells in different phases of cell cycle. In three independent experiments, cells expressing sNsp15 consistently had ca. 2 to 3% more cells in S phase compared to those transfected with the empty vector ($n = 3$, $P < 0.0001$; Fig. 5B). We note that the effects observed are likely to be underestimated due to the efficiency of transfection being <100%.

Finally, we examined whether sNsp15 could alter expression of *Renilla* luciferase driven from the thymidine kinase (TK) promoter, which is normally repressed by pRb (8). In this assay, an interaction between sNsp15 and pRb should increase TK promoter activity. An active-site mutant of sNsp15, H249A, was used in this experiment since expression of WT sNsp15 potentially could nonspecifically reduce reporter expression due to the endoribonuclease activity. The H249A mutant of sNsp15 increased *Renilla* luciferase levels in a concentration-dependent manner

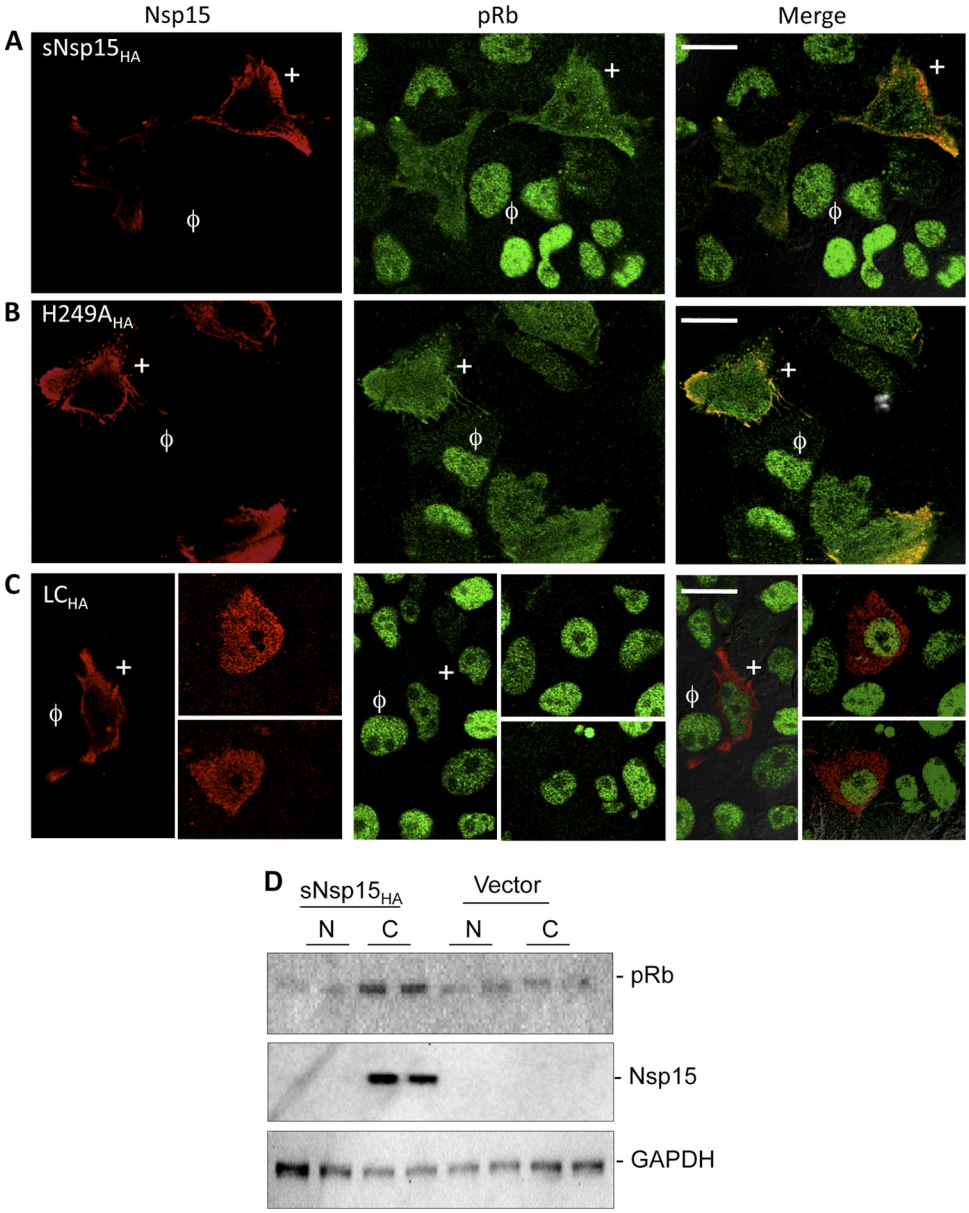

FIG 4 Distribution of pRb in cells expressing different forms of sNsp15. (A to C) Distribution of pRb (green) in Huh-7 cells transfected to express $sNsp15_{HA}$ (red) (A), $H249A_{HA}$ (B), and LC_{HA} (C). Due to the efficiency of transfection, each microscopic image contains both cells expressing sNsp15 and those that do not. To facilitate comparison of the images, a representative cell positive for WT or mutant sNsp15 is identified by a "+" symbol in all three sets of images. A typical cell that did not express WT or mutant sNsp15 is identified by the symbol "ϕ". In the presence of sNsp15, pRb is more diffused and colocalized to the cytoplasm with sNsp15. The three panels to the right show a merged image of pRb and Nsp15 staining. In panel C, a montage was prepared to increase the sample size due to the lower expression and/or transfection efficiency of LC_{HA}. The white scale bar in the lower right corner indicates 25 mm. (D) Western blot showing pRb levels (upper panel) in the nuclear (N) and cytoplasmic (C) fractions of transfected Huh7 cells. The middle panel shows the expression of Nsp15, as judged by probing the blot with anti-HA antibodies. GAPDH (glyceraldehyde-3-phosphate dehydrogenase) is shown as a loading control (lower panel).

(Fig. 5C). The same effects were not observed with luciferase expressed from a human cytomegalovirus (CMV) promoter that is not regulated by pRb. Altogether, the results from the NIH 3T3 focus formation, the proportions of cells in the S phase of the cell cycle, and the results from pRb-responsive promoter-reporter assay support the idea that the SARS-CoV Nsp15 can alter pRb regulation of cell growth and gene expression.

Nsp15 downregulates pRb accumulation. Several viral proteins that interact with pRb can accelerate its degradation (5, 21, 27). To determine whether this also takes place with sNsp15, the level of pRB_{ABC} was examined in transiently transfected 293T cells by Western blotting. In six independent assays, cells expressing WT sNsp15 had 3- to 4-fold lower amount of pRb compared to the vector control (Fig. 6A). The endoribonuclease-deficient mutant H249A also reduced pRb levels, although not to the same extent as the WT sNsp15 (Fig. 6A), indicating that reduction in pRb level by Nsp15 could be a combined effect of its endoribonuclease activity and enhanced protein degradation.

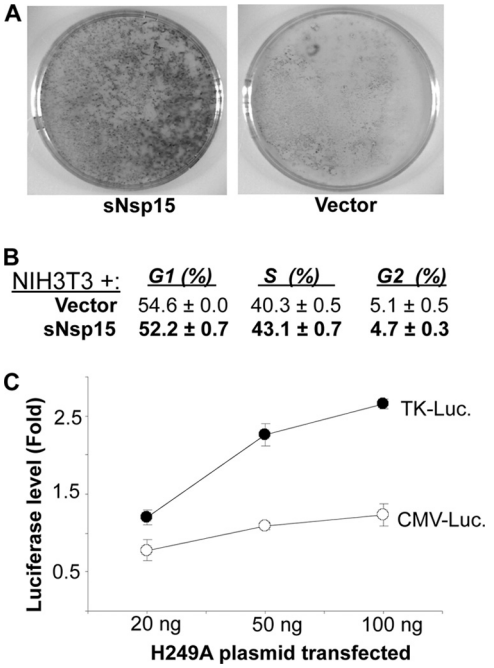

FIG 5 Effect of SARS Co-V Nsp15 on pRb-regulated processes. (A) Colony formation assay. The images show the growth of sNsp15- or vector-transfected NIH 3T3 cells. Colonies were stained with crystal violet. (B) Cell distribution in various phases of the cell cycle in vector or sNsp15-transfected cells as analyzed by FACS. (C) Effects of expressing H249A (endoribonuclease mutant of sNsp15) on luciferase expression from the thymidine kinase (TK) promoter (●) and the CMV promoter (○).

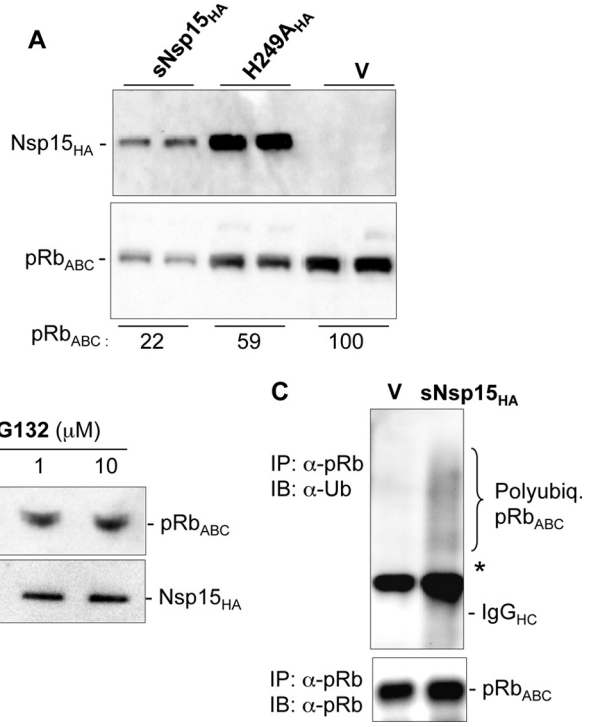

FIG 6 Cellular levels of pRb. (A) Western blot showing the expression levels of pRb_{ABC} in cells coexpressing either vector, $sNsp15_{HA}$, or $H249A_{HA}$. (B) Effect of proteasome inhibitor MG132 on the levels of pRb_{ABC} in the presence of $sNsp15_{HA}$. (C) Western blot showing the amount of ubiquitinated pRb in either vector (V)- or $sNsp15_{HA}$-transfected cells. Anti-pRb monoclonal antibodies were used for immunoprecipitation (IP), and anti-ubiquitin antibodies were used for Western blotting (IB) The expected position of pRb_{ABC} is indicated with a star. The blot was stripped and reprobed with anti-pRb antibodies (bottom panel).

pRb abundance has been shown to be regulated by several pathways, including ubiquitin-dependent proteolysis by the proteasome (39). To determine whether the reduction in pRb levels was due to enhanced proteolysis in the presence of sNsp15, we treated $sNsp15_{HA}$-transfected cells with the proteasome inhibitor MG132 and observed that pRb levels increased by up to 4-fold without affecting sNsp15 levels (Fig. 6B). This result suggests that the effect of sNsp15 on pRb accumulation involves the proteasome.

Next, we examined whether decreased pRb levels is correlated with increased ubiquitination. An antibody specific to pRb was used to immunoprecipitate the cell lysates and the precipitated material subjected to Western blotting with a monoclonal antibody to ubiquitin (Fig. 6C). In addition to the IgG used in the immunoprecipitation assay, a smear with extra density was found to emanate from a band of the mass corresponding to unmodified pRb, a finding consistent with the increased ubiquitination of pRb in the presence of sNsp15.

Interaction between pRb and Nsp15 is required for optimal MHV infection. To examine whether the interaction between Nsp15 and pRb is significant for virus infection in cell culture, we used MHV (strain A59) as a surrogate coronavirus. MHV is a suitable substitute for SARS-CoV since its Nsp15 protein (mNsp15) has a structure nearly identical to that of the SARS-CoV Nsp15 and an identical mechanism of cleavage (42). Furthermore, it has a pRb-binding sequence, and the endoribonuclease activity of the recombinant mNsp15 was also increased in the presence of pRb (Fig. 1A and 2B).

To disrupt the interaction between Nsp15 and pRb, we constructed a mutant MHV named vLC where two residues of the putative pRb-binding sequence (LWCNE) were mutated to alanines (AWANE; mutated residues underlined) using the reverse genetic system described by Yount et al. (43). Mutant vLC formed plaques on L2 cell line monolayers that were consistently reduced in their diameters to ca. 60% of those formed by WT MHV (Fig. 7A and B). The peak virus titer obtained by vLC was reduced between 5-fold and 1 log compared to the WT MHV in three experiments (Fig. 7C). These results suggest that the loss of interaction between pRb and mNsp15 is detrimental to optimal MHV infection.

pRb is redistributed and downregulated during MHV infection. We wanted to examine whether MHV infection would affect the accumulation and cellular distribution of pRb. L2 cells were infected either with WT or with vLC MHV at an MOI of ~1.0 for 4 h and examined by immunofluorescence microscopy. The cells were stained to detect pRb, as well as the MHV N protein. pRb was localized primarily in the nucleus of uninfected cells (Fig. 8A, upper panels). However, in the WT MHV-infected cells, a significant amount of pRb was also present in the cytoplasm (Fig. 8A, middle panels). A similar cytoplasmic distribution of pRb was not observed in cells that were infected with vLC (Fig. 8A, lower panels). In addition, most of the vLC-infected cells appeared to be larger in size than WT MHV-infected cells, and N protein was present both in the nucleus and in the cytoplasm, unlike WT

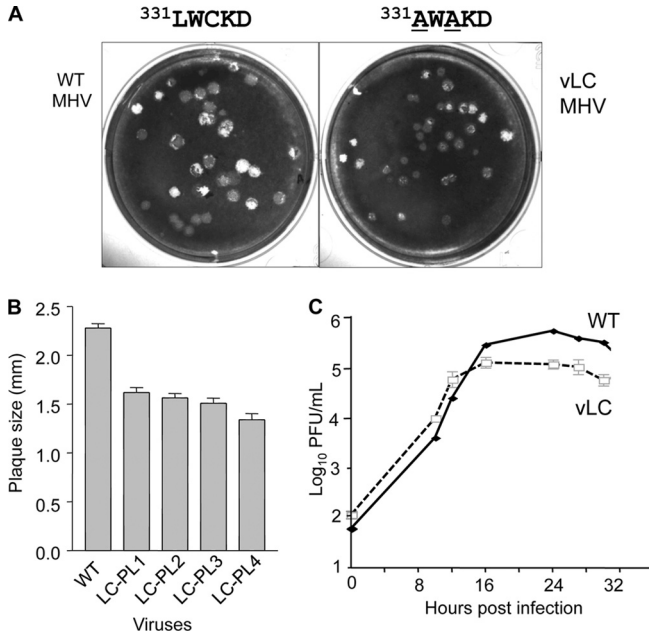

FIG 7 Plaque morphology and growth curve of vLC mutant MHV. (A) Representative plaque morphology of WT and vLC mutant MHV A59. (B) Diameter of plaques generated by four independent vLC mutant versus the WT MHV A59. (C) PFU generated by WT or vLC MHV as a function of time.

MHV-infected cells, where it was primarily cytoplasmic, a finding consistent with our previous observation that the LC mutant of the sNsp15 had pleiotropic effects on the physiology of the cells.

To examine pRb accumulation during MHV infection, L2 cells were infected with WT or vLC MHV or mock infected. The amounts of pRb in whole-cell lysates and cytoplasmic fractions were determined by Western blotting. Analysis of the whole-cell lysates shows that the amount of pRb was slightly lower in WT MHV- and vLC-infected cells compared to uninfected cells (Fig. 8B), whereas there was an ~2-fold-higher level of pRb in the cytoplasmic fractions of WT MHV-infected cells compared to uninfected or vLC-infected cells 1 hpi (Fig. 8C). These data demonstrate that MHV infection could increase pRb accumulation in the cytoplasm (Fig. 8). In addition, redistribution of pRb was observed as early as 1 h after MHV infection. There was an ~2-fold reduction in pRb accumulation and appearance of degradation product by WT MHV at 5 hpi. In contrast, the cytoplasmic pRb levels in cells infected with vLC remained apparently unaltered even by 5 hpi (Fig. 8C). The decrease in pRb levels by WT MHV infection by Western blot analysis was greater than that observed in the microscopy images, where pRb appears to be much brighter in the WT MHV infection (Fig. 8A). A potential explanation for this could be the detection of both partially degraded and full-length pRb in the microscopy experiments, while the Western blot results were for the full-length pRb. These results show that MHV infection is accompanied by pRb redistribution and downregulation, likely due to its interaction with Nsp15.

Effect of cellular levels of pRb on MHV infection. We reason that if pRb is downregulated during MHV infection, overexpression of pRb should negatively affect the MHV infection. Furthermore, overexpressing pRb should have less of an effect on the vLC mutant. To examine this possibility, we ectopically expressed pRb_{ABC} in DBT cells prior to infection by either WT or vLC MHV. Vector-transfected cells were used as a control. At the indicated times after infection, the cells were harvested to analyze the level of the MHV N protein by Western blotting. Cells with overexpressed pRb_{ABC} exhibited a delayed appearance of N protein by up to 2 h compared to the cells transfected with the empty vector (Fig. 9). Furthermore, pRb overexpression apparently did not affect N protein appearance in cells infected with vLC. Identical results were observed in two independent experiments. We note that the pRb_{ABC} levels were decreased by both WT and vLC MHV after 8 hpi (Fig. 9, bottom panels).

DISCUSSION

In this study, we found that Nsp15 can interact with pRb, increase expression of genes that are normally repressed by pRb, and increase the proportion of cells in the S phase of the cell cycle. The virus titer produced by an MHV with a mutation in Nsp15 that affected interaction with pRb was reduced by up to 1 log. Furthermore, overexpression of pRb in cells delayed the timing for N protein expression. These results support the idea that the coronaviruses can affect cell cycle-associated gene expression through a novel function of the putative endoribonuclease, Nsp15, likely to alter the metabolic status of the host cells to their advantage.

The effect of host metabolic status on virus replication was highlighted by the observation that transformed cells are better hosts for murine hepatitis coronavirus (40). Further, the importance of a coronavirus affecting cellular gene regulation through cell cycle progress is underscored by the Nsp1 protein of MHV, which has been reported to inhibit progression into the cell cycle at the G_0/G_1 transition by decreasing Cdk1 levels and accumulating hypophosphorylated pRb (6). Since the LXCXD/E motif binds preferentially to hypophosphorylated pRb (23), it is conceivable that Nsp1 accumulates the hypophosphorylated form of pRb for interaction with Nsp15.

Our observations of increased relocalization of pRb to the cytoplasm and association with ubiquitin indicate that a consequence of the interaction with Nsp15 is the degradation of pRb, likely by the ubiquitin/proteasome pathway. The proteins tumor suppressor p53 and $p27^{Kip1}$ are also redistributed to the cytoplasm for their degradation (14, 19). We note with interest that Nsp15 lacking the WT pRb-binding site (sLC) accumulates to lower levels and has significant cytotoxicity, suggesting that interaction with pRb stabilizes Nsp15 and has other consequences for viral infection. It is not yet clear why Nsp15 appears to require pRb for its own stability and enhances the downregulation of pRb. However, the observed effects on pRb-regulated processes and gene expression are likely due to a direct protein interaction since pRb can coimmunoprecipitate with Nsp15 and increase the endoribonuclease activity. Furthermore, we note with interest that Nsp15 lacking the wild-type pRb-binding site had significant cytotoxicity, suggesting that interaction with pRb has other consequences for viral infection.

Especially important to MHV infection is that an effect on pRb was observed by 1 h after infection, suggesting that debilitating pRb is an early event in infection (Fig. 8 and 9). We also observed a dramatic reduction in pRb_{ABC} levels after 8 hpi (Fig. 9) during the infection by both WT and vLC MHV. This effect is probably due to the host translational shutoff induced by MHV. Although a mutation to prevent Nsp15 and pRb interaction only reduced MHV virion production by up to 1 log in a single round of infec-

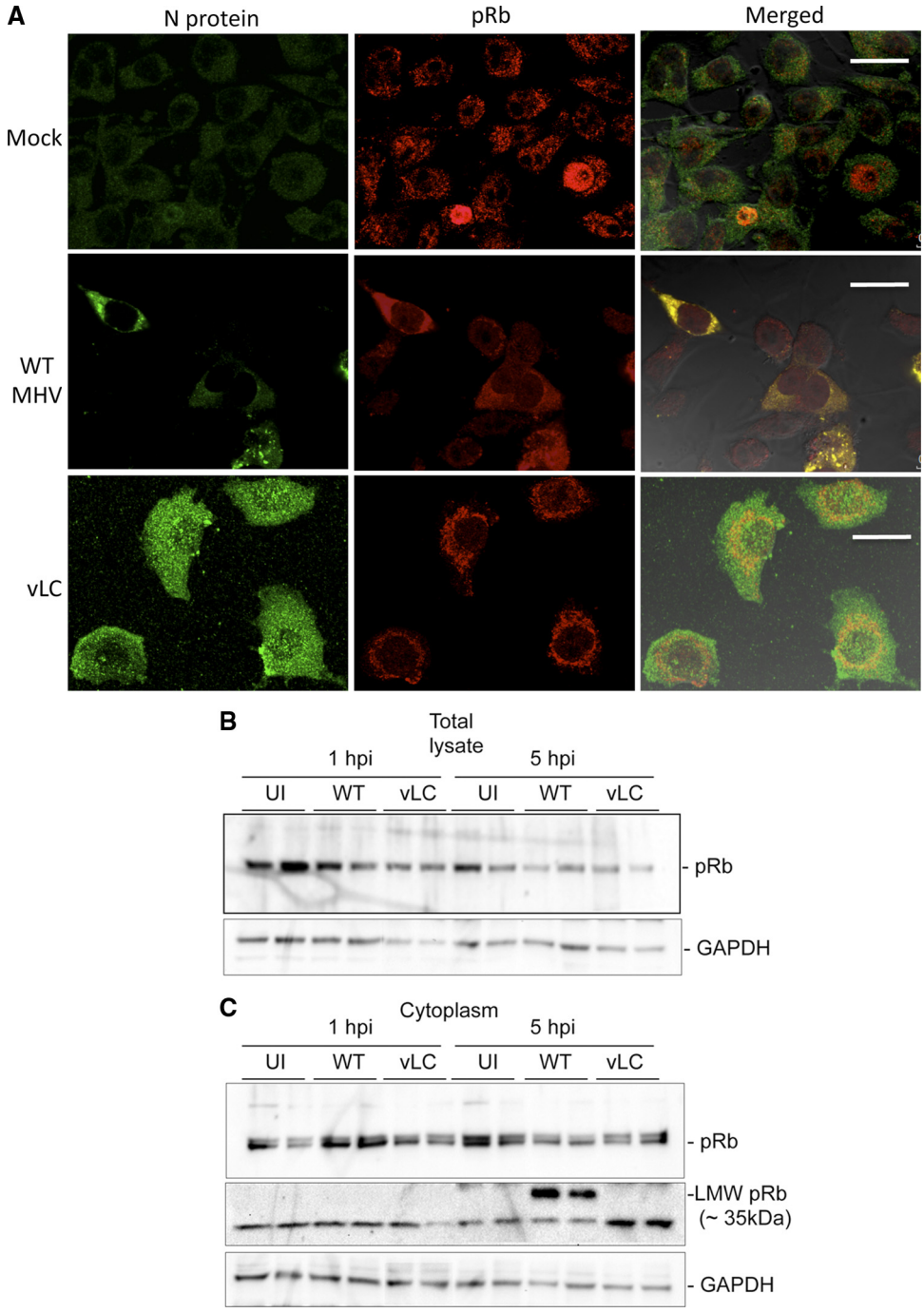

FIG 8 Distribution and levels of pRb during MHV infection. (A) Confocal microscopy images of L2 cells showing the distribution of pRb (red) and MHV N protein (green) in untreated cells (top panels), WT MHV-infected cells (middle panels), and vLC MHV-infected cells (lower panels). Right panels show a merged image of pRb and N protein staining. pRb is stained with rabbit anti-mouse antibody and Texas Red conjugated anti-rabbit secondary antibody. N protein is stained with anti-MHV N protein monoclonal antibodies and Alexa Fluor 488-conjugated anti-mouse secondary antibody. The white scale bar in the right panels indicates 25 μm. (B) Western blots showing the levels of pRb in whole cells lysates (top panel). The level of GAPDH was used as a loading control (bottom panel). (C) Western blots showing the levels of pRb in the cytoplasmic fraction (top and middle panels). GAPDH (bottom panel) serves as a loading control. L2 cells were infected either with WT or vLC MHV. Cells were harvested 1 or 5 hpi. Uninfected cells (UI) were used as a control. Western blots are probed with anti-pRb antibodies in panels B and C.

tion, it is likely to have a much more dramatic effect in a host organism during multiple rounds of infection. Further, pRb interacts with several cellular proteins and regulates the expression of multiple genes, including those associated with the cell cycle (32), and immune response genes, including those associated with interleukin-6 (IL-6) and IL-8 (7, 44). DNA tumor viruses and HCV are linked to cancer, and interaction with pRb provides one mechanism to alter regulation of cell cycle progression. Coronaviruses

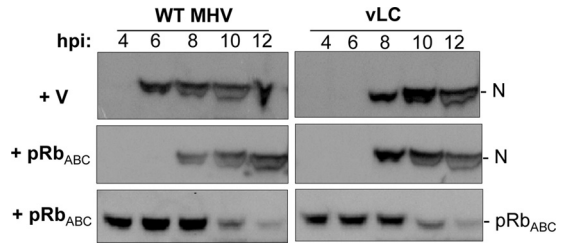

FIG 9 Effect of pRb overexpression on MHV infection. The Western blot shows the level of viral nucleocapsid (N) and pRb_{ABC} protein expressed in DBT cells transfected either with vector (+V) or pRb_{ABC} (+pRb_{ABC}) and subsequently infected with either WT (left panels) or vLC MHV (right panels). The times of sample collection are shown above the Western blot image. The MHV N protein was detected with anti-MHV N protein monoclonal antibodies and horseradish peroxidase-conjugated anti-mouse secondary antibody. pRb was detected with monoclonal anti-human pRb antibodies and horseradish peroxidase-conjugated anti-mouse secondary antibody.

are not known to be associated with cancer, but perturbing cell cycle regulation will affect the metabolism of the cell and the accumulation of gene products to favor optimal viral infection.

We observed that many, but not all members of the alpha and beta coronaviruses contain a Rb-binding motif on their endoribonuclease (Fig. 1A). Interestingly, members of gamma coronavirus genus and related nidoviruses lack an LXCXE/D sequence on their orthologs of Nsp15. However, such motifs can be found in other protein in open reading frame 1ab. This suggests that interaction with Rb may be important, although endoribonuclease activity does not require this interaction. The functional relevance of the observed motifs in other nidoviruses needs to be investigated directly prior to making any conclusions about the specific requirements of Rb interaction in the infection process.

ACKNOWLEDGMENTS

C.C.K. acknowledges partial support from NIH 1R01AI090280. J.L.L. acknowledges support from NIH AI067416.

REFERENCES

1. **Atreya CD, et al.** 1998. The rubella virus putative replicase interacts with the retinoblastoma tumor suppressor protein. Virus Genes **16**:177–183.
2. **Bhardwaj K, Guarino L, Kao CC.** 2004. The severe acute respiratory syndrome coronavirus Nsp15 protein is an endoribonuclease that prefers manganese as a cofactor. J. Virol. **78**:12218–12224.
3. **Bhardwaj K, et al.** 2008. Structural and functional analyses of the severe acute respiratory syndrome coronavirus endoribonuclease Nsp15. J. Biol. Chem. **283**:3655–3664.
4. **Bhardwaj K, Sun J, Holzenburg A, Guarino LA, Kao CC.** 2006. RNA recognition and cleavage by the SARS coronavirus endoribonuclease. J. Mol. Biol. **361**:243–256.
5. **Boyer SN, Wazer DE, Band V.** 1996. E7 protein of human papillomavirus-16 induces degradation of retinoblastoma protein through the ubiquitin-proteasome pathway. Cancer Res. **56**:4620–4624.
6. **Chen CJ, Sugiyama K, Kubo H, Huang C, Makino S.** 2004. Murine coronavirus nonstructural protein p28 arrests cell cycle in G_0/G_1 phase. J. Virol. **78**:10410–10419.
7. **Chen PL, Riley DJ, Chen-Kiang S, Lee WH.** 1996. Retinoblastoma protein directly interacts with and activates the transcription factor NF-IL6. Proc. Natl. Acad. Sci. U. S. A. **93**:465–469.
8. **Coppock DL, Pardee AB.** 1987. Control of thymidine kinase mRNA during the cell cycle. Mol. Cell. Biol. **7**:2925–2932.
9. **DeCaprio JA, et al.** 1988. SV40 large tumor antigen forms a specific complex with the product of the retinoblastoma susceptibility gene. Cell **54**:275–283.
10. **DeGregori J, Kowalik T, Nevins JR.** 1995. Cellular targets for activation by the E2F1 transcription factor include DNA synthesis- and G_1/S-regulatory genes. Mol. Cell. Biol. **15**:4215–4224.
11. **Dyson N, Howley PM, Munger K, Harlow E.** 1989. The human papillomavirus-16 E7 oncoprotein is able to bind to the retinoblastoma gene product. Science **243**:934–937.
12. **Enjuanes L, et al.** 2006. Biochemical aspects of coronavirus replication. Adv. Exp. Med. Biol. **581**:13–24.
13. **Forng RY, Atreya CD.** 1999. Mutations in the retinoblastoma protein-binding LXCXE motif of rubella virus putative replicase affect virus replication. J. Gen. Virol. **80**(Pt 2):327–332.
14. **Freedman DA, Levine AJ.** 1998. Nuclear export is required for degradation of endogenous p53 by MDM2 and human papillomavirus E6. Mol. Cell. Biol. **18**:7288–7293.
15. **Freundt EC, Yu L, Park E, Lenardo MJ, Xu XN.** 2009. Molecular determinants for subcellular localization of the severe acute respiratory syndrome coronavirus open reading frame 3b protein. J. Virol. **83**:6631–6640.
16. **Guarino LA, et al.** 2005. Mutational analysis of the SARS virus Nsp15 endoribonuclease: identification of residues affecting hexamer formation. J. Mol. Biol. **353**:1106–1117.
17. **Holmes KV, Enjuanes L.** 2003. Virology—the SARS coronavirus: a post-genomic era. Science **300**:1377–1378.
18. **Ivanov KA, et al.** 2004. Major genetic marker of nidoviruses encodes a replicative endoribonuclease. Proc. Natl. Acad. Sci. U. S. A. **101**:12694–12699.
19. **Kamura T, et al.** 2004. Cytoplasmic ubiquitin ligase KPC regulates proteolysis of $p27^{Kip1}$ at G_1 phase. Nat. Cell Biol. **6**:1229–1235.
20. **Kang H, et al.** 2007. Biochemical and genetic analyses of murine hepatitis virus Nsp15 endoribonuclease. J. Virol. **81**:13587–13597.
21. **Kim HY, Ahn BY, Cho Y.** 2001. Structural basis for the inactivation of retinoblastoma tumor suppressor by SV40 large T antigen. EMBO J. **20**:295–304.
22. **Lai MM, Cavanagh D.** 1997. The molecular biology of coronaviruses. Adv. Virus Res. **48**:1–100.
23. **Lee JO, Russo AA, Pavletich NP.** 1998. Structure of the retinoblastoma tumour-suppressor pocket domain bound to a peptide from HPV E7. Nature **391**:859–865.
24. **Lei Y, et al.** 2009. MAVS-mediated apoptosis and its inhibition by viral proteins. PLoS One **4**:e5466.
25. **Masters PS.** 2006. The molecular biology of coronaviruses. Adv. Virus Res. **66**:193–292.
26. **Moran E.** 1993. DNA tumor virus transforming proteins and the cell cycle. Curr. Opin. Genet. Dev. **3**:63–70.
27. **Munakata T, et al.** 2007. Hepatitis C virus induces E6AP-dependent degradation of the retinoblastoma protein. PLoS Pathog. **3**:1335–1347.
28. **Munakata T, Nakamura M, Liang Y, Li K, Lemon SM.** 2005. Down-regulation of the retinoblastoma tumor suppressor by the hepatitis C virus NS5B RNA-dependent RNA polymerase. Proc. Natl. Acad. Sci. U. S. A. **102**:18159–18164.
29. **Munger K, et al.** 1989. Complex formation of human papillomavirus E7 proteins with the retinoblastoma tumor suppressor gene product. EMBO J. **8**:4099–4105.
30. **Naniche D, Reed SI, Oldstone MB.** 1999. Cell cycle arrest during measles virus infection: a G_0-like block leads to suppression of retinoblastoma protein expression. J. Virol. **73**:1894–1901.
31. **Nelson HB, Tang H.** 2006. Effect of cell growth on hepatitis C virus (HCV) replication and a mechanism of cell confluence-based inhibition of HCV RNA and protein expression. J. Virol. **80**:1181–1190.
32. **Nevins JR.** 1992. E2F: a link between the Rb tumor suppressor protein and viral oncoproteins. Science **258**:424–429.
33. **Nga PT, et al.** 2011. Discovery of the first insect nidovirus, a missing evolutionary link in the emergence of the largest RNA virus genomes. PLoS Pathog. **7**:e1002215.
34. **Pietschmann T, Lohmann V, Rutter G, Kurpanek K, Bartenschlager R.** 2001. Characterization of cell lines carrying self-replicating hepatitis C virus RNAs. J. Virol. **75**:1252–1264.
35. **Posthuma CC, et al.** 2006. Site-directed mutagenesis of the nidovirus replicative endoribonuclease NendoU exerts pleiotropic effects on the arterivirus life cycle. J. Virol. **80**:1653–1661.
36. **Ricagno S, et al.** 2006. Crystal structure and mechanistic determinants of SARS coronavirus nonstructural protein 15 define an endoribonuclease family. Proc. Natl. Acad. Sci. U. S. A. **103**:11892–11897.

37. **Rota PA, et al.** 2003. Characterization of a novel coronavirus associated with severe acute respiratory syndrome. Science **300**:1394–1399.
38. **Scholle F, et al.** 2004. Virus-host cell interactions during hepatitis C virus RNA replication: impact of polyprotein expression on the cellular transcriptome and cell cycle association with viral RNA synthesis. J. Virol. **78**:1513–1524.
39. **Sdek P, et al.** 2005. MDM2 promotes proteasome-dependent ubiquitin-independent degradation of retinoblastoma protein. Mol. Cell **20**:699–708.
40. **Sturman LS, Takemoto KK.** 1972. Enhanced growth of a murine coronavirus in transformed mouse cells. Infect. Immun. **6**:501–507.
41. **Whyte P, et al.** 1988. Association between an oncogene and an anti-oncogene: the adenovirus E1A proteins bind to the retinoblastoma gene product. Nature **334**:124–129.
42. **Xu X, et al.** 2006. New antiviral target revealed by the hexameric structure of mouse hepatitis virus nonstructural protein nsp15. J. Virol. **80**:7909–7917.
43. **Yount B, Denison MR, Weiss SR, Baric RS.** 2002. Systematic assembly of a full-length infectious cDNA of mouse hepatitis virus strain A59. J. Virol. **76**:11065–11078.
44. **Zhang H, et al.** 2000. Retinoblastoma protein activation of interleukin 8 expression inhibits tumor cell survival in nude mice. Cell Growth Differ. **11**:635–639.